Dill, R., Dobslaw, H. (2019): Seasonal Variations in Global Mean Sea-Level and Consequences on the Excitation of Length-of-Day Changes. - *Geophysical Journal International*, *218*, 2, pp. 801—816.

DOI: http://doi.org/10.1093/gji/ggz201

Geophysical Journal International

Geophys. J. Int. (2019) **218,** 801–816
Advance Access publication 2019 April 29
GJI Gravity, Geodesy and Tides

doi: 10.1093/gji/ggz201

Seasonal variations in global mean sea level and consequences on the excitation of length-of-day changes

R. Dill and H. Dobslaw

Earth System Modelling, GFZ German Research Centre for Geosciences, Helmholtz Centre Potsdam, 14473 Potsdam, Germany. E-mail: dill@gfz-potsdam.de

Accepted 2019 April 27. Received 2019 April 25; in original form 2019 March 6

SUMMARY

Global mass redistribution between the Earth subsystems oceans, atmosphere and continental hydrosphere causes a predominantly seasonal signal in Earth rotation excitation that superimposes the effects of each individual Earth subsystem. Especially for annual length-of-day variations a consistent consideration of the global mass balance among atmosphere, ocean and continental water is necessary to compare the simulated effective angular momentum functions for Earth rotation from geophysical models with geodetic observations. In addition to atmospheric, oceanic and hydrological contributions, we estimate the contributions due to the global mass balance effect using the new ESMGFZ SLAM product as well as estimates of the barystatic ocean bottom pressure anomalies from the GRACE Level 3 GravIS products. For the annual cycle the global mass balance effect overcompensates the contributions to length-of-day variations from terrestrial hydrology. Moreover, most of the atmospheric surface pressure contribution is also compensated. The global mass balance effect has to be calculated for each combination of geophysical Earth system models individually. Considering the global mass balance, model based mass induced excitation on seasonal length-of-day variations coincide well with estimates from satellite gravimetry. Moreover, the mass terms can be determined accurate enough to attribute the remaining gap in the length-of-day excitation budget between models and observation clearly to an underestimation of atmospheric wind speeds in the global European weather forecast model. Magnifying its wind speeds by +7 per cent the sum of all ESMGFZ angular momentum functions can almost perfectly explain the total length-of-day excitation.

Key words: Earth's rotation variations; Sea level change; Satellite geodesy; Satellite gravity; Reference systems.

1 INTRODUCTION

On seasonal timescales, changes in Earth's rotational speed expressed as length-of-day variations (ΔLOD) are mainly caused by external gravitational forces, the redistribution of water masses within Earth's fluid layers, atmosphere, ocean and terrestrial hydrosphere and the exchange of water masses between these components. Models of the hydrosphere dynamics, that is, numerical weather prediction models, ocean general circulation models and terrestrial water storage models can be used to calculate forced Earth rotational variations, the so-called Earth rotation excitation functions or effective angular momentum (EAM) functions. Atmospheric winds and surface pressure changes, atmospheric angular momentum (AAM) account for almost 90 per cent of the observed changes in ΔLOD (e.g. Gross *et al.* 2004). To a smaller extent ΔLOD is excited by terrestrial hydrology (HAM). In particular, large-scale variations in water masses on the continents and the exchange of water masses between the continents and the ocean are responsible for the seasonal signal in Earth's rotational speed.

Whereas many individual model-based EAM time-series for the atmosphere, ocean and continental hydrology are analysed, compared and even combined in great detail (e.g. Brzezinski 1992; Chen & Wilson 2005; Zhou *et al.* 2005; Brzezinski *et al.* 2009; Chen *et al.* 2012; Nastula *et al.* 2012), the effect of global mass conservation among different model combinations has been often neglected, most likely due to the absence of adequate data products. The International Earth Rotation and Reference Systems Service (IERS) provides a comprehensive list of publicly available AAM, OAM, HAM time-series but the global mass conservation among the underlying Earth system models is generally not ensured. In order to analyse the total Earth excitation budget (AAM+OAM+HAM) the global mass balance effect (GMB) has to be calculated additionally by the user itself, especially for seasonal excitation studies. Unfortunately, the necessary seasonal variations in total atmospheric,

oceanic and terrestrial water storage of the Earth system models are commonly not provided along with the EAM functions. Only a few studies explicitly analysed the GMB. Chao *et al.* (1988) described explicit formulas for the sea-level correction in gravity and polar motion that are necessary to conserve global water mass. In addition to AAM calculated from NCEP reanalysis (National Centers for Environmental Prediction), OAM calculated from the ocean model data ECCO (Estimating the Circulation and Climate of the Ocean) and HAM from the U.S. Climate Prediction Center (CPC) land data assimilation system model, Chen (2005) calculated a coherent mass balance among these models. The mass balancing effects, especially from the balance between land and ocean, nearly completely cancelled the model predicted HAM excitations. The authors compared also two different mass balancing methods. Based on the modelled terrestrial water storage and the atmospheric mass a global and an oceanic balance of the total excess mass was applied. There was no significant difference between these two approaches. More recently, Yan *et al.* (2012) calculated the effect of global mass conservation on the seasonal length of day variation for the individual contributions of the geophysical fluids using atmospheric surface pressure from ECMWF (European Centre for Medium-Range Weather Forecasts) for the atmosphere, ocean bottom pressure from ECCO and terrestrial water storage from GLDAS (Global Land Data Assimilation System). Taking the GMB into account the combined mass-induced excitations of ΔLOD by geophysical fluids was in much better agreement with that observed by Satellite Laser Ranging (SLR). Yu *et al.* (2018) fitted a weighted mean wavelet combination of several narrow-frequency-band components from different geophysical models to an SLR solution in order to pick up the most reliable signals out of many modelled EAM data sets. Assuming that the atmospheric motion terms are determined the best, their results indicate model deficiencies mainly in the ocean excitation, but they do not discuss processes such as GMB and self-attraction as these effects are generally not included in the available EAM data sets. However, the GMB is inseparably related to the applied atmospheric and hydrological models and should be estimated specifically for every combination of geophysical fluid models.

Since the beginning of 2017 the Earth System Modelling group at GFZ Potsdam (ESMGFZ) provides so-called barystatic Sea-Level Angular Momentum functions (SLAM) that account for the GMB consistent to their models used for the calculation of AAM, OAM and HAM products (Dobslaw *et al.* 2010). In contrast to this purely model-based estimates of the geophysical fluids excitations of polar motion and ΔLOD, the Gravity Information Service website http://gravis.gfz-potsdam.de/ (GravIS), launched in 2018 by GFZ provides a preliminary separation of the ocean gravity signal observed by GRACE into the part induced by general circulation pressure anomalies and the GMB part induced by barystatic pressure anomalies. From the latter mass distribution we can derive a SLAM product that relies almost purely on observations from the Gravity Recovery and Climate Experiment (GRACE). Both products, SLAM from ESMGFZ models and from GRAVIS, are fully consistent with the new GRACE release 06. In this study we will assess the GMB effect in Earth rotation from these two new operational products and use it to close the total excitation budget. The total excitation of ΔLOD can be divided into a mass term induced by mass redistribution and a motion term induced by mass movements like atmospheric winds and ocean currents. In addition to the modelled excitation, the mass term can be also assessed from the degree-two coefficients of the global gravitational potential observed by geodetic satellite missions like SLR and GRACE. There exist no analogous direct observations of the motion term. Assuming that the mass term can be determined with sufficient accuracy, an indirectly observed or pseudo-observed motion term can be derived by subtracting the defined mass term from observation of the total geodetic excitation. This geodetic angular momentum function (GAM) for ΔLOD is simply the time derivative of the observed variation in Earth's length-of-day. Since the oceanic motion term is known to be almost two magnitudes smaller than the atmospheric motion term, the comparison of the modelled atmospheric motion term with the pseudo-observed motion term provides indications about the quality of atmospheric winds predicted by global weather models.

Please consult the list of acronyms (Table 3) for the nomenclature of the different angular momentum functions and their producers.

2 BARYSTATIC SEA-LEVEL CHANGES

Barystatic sea-level changes are induced by (i) the net-inflow of water from the continents or the atmosphere into the oceans, and (ii) by a spatially variable deformation of an equipotential surface of the Earth's gravity field that coincides with the sea-surface on a global average. Ocean mass variations are either inferred from a combination of satellite altimetry and oceanographic *in situ* observations, or more directly from the satellite gravity missions GRACE (2002–2017) and GRACE-FO (launched on 2018 May 22). From the latest GRACE reprocessing release 06 performed at GFZ (Dahle *et al.* 2018), publicly available via the GravIS portal (gravis.gfz-potsdam.de), we find that global mean sea level varies with an annual amplitude of 8.80 mm and rises at average rate of 0.87 mm per year when estimated for the period 2003–2016 after applying a global model of glacial isostatic adjustment (Klemann *et al.* 2008).

Alternatively, barystatic sea-level changes might be also inferred from the knowledge of the global hydrospheric mass distributions away from the continents. In terms of its global mass, Earth is an almost perfectly closed system that exchanges mass with the extraterrestrial space at very small rates only. In terms of the global water cycle in particular, the total mass of water on the globe can be safely assumed to be constant in time. Gravitationally consistent spatially heterogeneous sea-level variations can be deduced by solving the so-called sea-level equation (Tamisiea *et al.* 2010). Based on daily estimates of the ESMGFZ models of the atmosphere (i.e. global ECMWF analysis and re-analysis data) and the continental hydrosphere (i.e. Land Surface Discharge Model, LSDM), we note that, apart from the trend, both signals agree very well even on interannual timescales (Fig. 1). The annual amplitude of the barystatic sea-level changes inferred from the ESMGFZ models is about 5 per cent higher than the most recent GRACE estimate from GFZ, and the phase difference is about 7 d. ESMGFZ does not account for post-glacial rebound.

3 EFFECTIVE ANGULAR MOMENTUM FUNCTIONS

EAM functions (χ_1, χ_2, χ_3) summarize the excitation of Earth orientation changes due to mass redistribution and mass movement by means of the Liouville equation (e.g. Barnes *et al.* 1983; Brzezinski 1992). The equatorial EAM χ_1 and χ_2 excite polar motion, whereas the axial component χ_3 quantifies ΔLOD by

$$\Delta\mathrm{LOD} = -\mathrm{LOD} \cdot (\chi_3^{\mathrm{mass}} + \chi_3^{\mathrm{motion}}) \quad (1)$$

with LOD=86400s. Each EAM function consists of so-called mass terms induced by mass redistributions, and motion terms caused

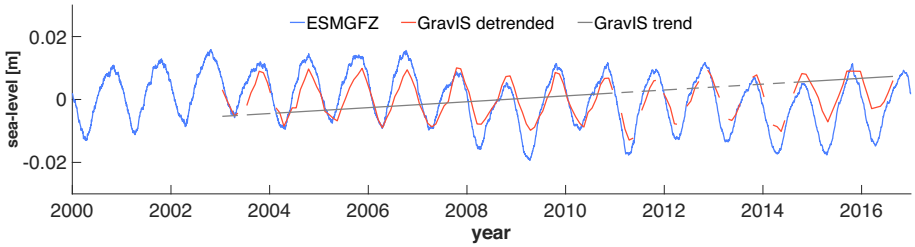

Figure 1. Barystatic sea-level variations for the years 2000–2016 in [m]. Blue: 24-hourly sea level calculated from atmospheric and hydrological mass changes in the ESMGFZ models ECMWF and LSDM by solving the sea-level equation. Red: Monthly GRACE based sea-level variation from GravIS Barystatic Pressure Anomalies, detrended. Grey: removed trend of GravIS Barystatic Pressure Anomalies.

by mass transports associated with atmospheric winds and ocean currents. Global numerical models allow for the separate quantification of angular momentum changes due to atmospheric variability (AAM), ocean dynamics (OAM), terrestrial water cycle variations (HAM), barystatic sea-level changes (SLAM) and further processes associated with mass shifts in the cryosphere and the solid Earth. Alternatively, satellite geodesy allows for the quantification of the total excitation from the inversion of the Earth orientation parameters as available from in particular geometric techniques, and additionally also for the estimation of the total mass term from the analysis of gravimetric observations.

3.1 Model-based AAM and OAM from ESMGFZ

Since more than 10 yr, ESMGFZ provides daily updated EAM functions as calculated from numerical weather model data provided by the ECMWF. Atmospheric surface pressure from the global reanalyses ERA-40 (1976–1978), ERA-Interim (1979–2006) and operational numerical weather prediction data (from 2007 onwards) are projected onto a time-invariant reference topography (Dobslaw 2016) to obtain a long-term stable AAM time-series. The IB correction is applied to surface pressure for all oceanic locations of the underlying 0.5° grid. Winds are evaluated at the original model level that smoothly follow the topography near the surface and align to isobaric surface in the middle atmosphere and above. Atmospheric tides at in total 12 frequencies are estimated and removed from the data and provided separately. The non-tidal AAM are provided with a temporal sampling of 3 hr.

OAM are calculated from ocean bottom pressure and ocean currents of an unconstrained simulation with the Max-Planck-Institute for Meteorology Ocean Model (MPIOM; Jungclaus *et al.* 2013) forced with the same atmospheric data from ECMWF as used for the AAM. The additive-inverse IB correction is applied to ocean bottom pressure, and the oceanic response to atmospheric tides has been estimated and removed from both mass and motion terms. OAM are available with the same temporal sampling and at the same epochs as the AAM described above.

It is worth mentioning here that the current version of AAM and OAM provided by ESMGFZ is consistent with the GRACE Non-Tidal Atmosphere and Ocean De-Aliasing Level-1B (AOD1B) Product in its latest Release 06 (Dobslaw & Dill 2017) in terms of the underlying mass distributions and the handling of atmospheric tides. ESMGFZ intends to maintain this consistency also for future updates of AOD1B during the upcoming years of the GRACE-FO mission.

3.2 Model-based HAM and SLAM from ESMGFZ

EAM functions of the terrestrial hydrosphere (HAM) are calculated from terrestrial water storage as simulated with the LSDM (Dill 2008). Model-derived water storage includes snow accumulation, seasonal runoff from glaciers and water flow in river channels given as daily states on a 0.5° regular global grid. Physics and parametrization of LSDM are based on the hydrological discharge model (HDM; Hagemann & Dümenil 1998a) and the Simplified Land Surface Scheme (SLS; Hagemann & Dümenil 1998b, 2003). LSDM represents soil moisture, lakes, snow and ice as bucket-like surface reservoirs generating excess runoff and drainage depending on the saturation-capacity ratios. Runoff and drainage are passed down by the model river network as overland flow, base flow and river flow. The retention and translation of water in each flow process is described by a two-parameter approach representing a cascade of equal linear reservoirs with individual retention time coefficients. LSDM is forced with atmospheric data at high spatial and temporal resolution obtained consistently from the corresponding ECMWF models used for AAM and OAM.

SLAM data is calculated from the global distributions of ECMWF atmospheric and LSDM terrestrial water storage masses by means of the sea-level equation (Tamisiea *et al.* 2010). SLAM thus balances the global mass in the model system in a way that the sum of the total mass in all four different EAM components (i.e. AAM, OAM, HAM and SLAM) is constant at any time. SLAM represents mainly the hydrological and atmospheric excess mass distributed globally into the ocean but includes also the gravimetric effect of loading and self-attraction acting on the ocean sea level. Note that ocean volume is implicitly maintained in MPIOM by means of the Boussinesq approximation, and a spatially uniform correction is applied at every time-step to adjust for thereby induced fluctuations in ocean mass (Greatbatch 1994). For completeness, we note that in OAM products available from ESMGFZ until the end of 2017 (Dobslaw *et al.* 2010), the effects of time-variations in the total ocean mass that are now represented by SLAM were included in the OAM mass term. Since most ocean general circulation models available for Earth orientation studies do not include variations in ocean mass, ESMGFZ separates now the contributions from the ocean domain into a part caused by internal ocean dynamics (OAM) and the part caused by barystatic sea-level variations (SLAM). That way OAM time-series are comparable among different ocean models.

All EAM data sets calculated by ESMGFZ are available since January 1976 with daily (HAM, SLAM) or even three-hourly (AAM, OAM) sampling and thus span over a time-period of more than four decades. All data, technical documentation and latest news are available from esmdata.gfz-potsdam.de:8080.

Table 1. Seasonal signal in χ_3 mass term.

	Annual		Semi-annual	
	Amplitude (10^{-10})	Phase (deg)	Amplitude (10^{-10})	Phase (deg)
AAM mass				
ESMGFZ (ECMWF)	4.23 ± 0.02	199.83 ± 0.28	0.99 ± 0.02	114.12 ± 1.18
TUV (ECMWF)	4.73 ± 0.03	199.75 ± 0.37	1.02 ± 0.03	120.81 ± 1.71
AER (NCEP)	4.73 ± 0.03	201.87 ± 0.37	1.13 ± 0.03	110.05 ± 1.57
GravIS model AOD1B atmosphere	4.49 ± 0.23	204.01 ± 2.84	0.88 ± 0.03	128.96 ± 14.6
YAN (ECMWF)	4.16 ± 0.46	207.00 ± 1.00	0.72 ± 0.46	113.00 ± 3.00
OAM mass				
ESMGFZ (MPIOM)	2.08 ± 0.01	193.02 ± 0.41	0.54 ± 0.01	142.29 ± 1.56
GravIS model AOD1B ocean	2.22 ± 0.12	197.26 ± 3.16	0.59 ± 0.12	143.91 ± 12.0
GravIS model + res. circulation + leakage	3.40 ± 0.18	202.79 ± 2.96	1.26 ± 0.18	96.55 ± 7.99
JPL (ECCO)	0.84 ± 0.03	191.96 ± 1.78	0.35 ± 0.03	182.03 ± 4.35
YAN (ECCO)	1.04 ± 0.01	226.00 ± 0.00	0.42 ± 0.01	167.00 ± 2.00
HAM mass				
ESMGFZ (LSDM)	9.38 ± 0.07	99.10 ± 0.41	1.74 ± 0.07	150.74 ± 2.21
GravIS water storage + Ice	6.36 ± 0.28	107.64 ± 11.5	0.89 ± 0.28	147.48 ± 33.1
YAN (GLDAS)	6.35 ± 0.06	77.00 ± 1.00	0.95 ± 0.06	112.00 ± 3.00
SLAM				
ESMGFZ	11.71 ± 0.05	278,95 ± 0.26	1.55 ± 0.05	339,91 ± 1.96
GravIS barystatic sea level	8.31 ± 0.22	293,80 ± 1.51	0.33 ± 0.22	318,49 ± 38.1
YAN	9.17 ± 0.07	260.00 ± 1.00	1.06 ± 0.07	301.00 ± 3.00
contribution from Atm. balance				
ESMGFZ (ECMWF)	2.27 ± 0.01	51.85 ± 0.09	0.31 ± 0.02	212.50 ± 0.82
YAN (ECMWF)	1.88 ± 0.01	12.00 ± 1.00	0.59 ± 0.01	262.00 ± 1.00
contribution from Hydr. balance				
ESMGFZ (LSDM)	11.66 ± 0.05	270,66 ± 0.26	1.65 ± 0.05	1.02 ± 1.90
YAN (GLDAS)	10.09 ± 0.07	250.00 ± 0.00	0.72 ± 0.06	335.00 ± 0.00
contribution from Loading/self-attraction				
ESMGFZ (ECMWF+LSDM)	0.29 ± 0.11	211.09 ± 0.53	0.13 ± 0.11	141.52 ± 3.91
HAMmass + SLAM				
ESMGFZ	2.33 ± 0.12	278.35 ± 0.68	0.32 ± 0.12	100.84 ± 4.17
GravIS	1.95 ± 0.50	297.57 ± 13.0	0.57 ± 0.50	152.68 ± 71.2
YAN	2.85 ± 0.13	266.70 ± 2.00	0.19 ± 0.13	351.69 ± 6.00
GRACE/SLR HAM+SLAM				
GFZ RL06-SLR_GFZ	3.11 ± 0.20	276,80 ± 3.70	1.34 ± 0.20	99.71 ± 8.58
GFZ RL06-SLR_TN11	3.88 ± 0.21	260.88 ± 3.09	1.30 ± 0.21	94.49 ± 9.18
SLR_TN11	3.69 ± 0.20	262.07 ± 3.13	1.66 ± 0.20	92.95 ± 6.92
AAMmass + OAMmass + HAMmass + SLAM				
ESMGFZ	7.06 ± 0.16	216.67 ± 1.36	1.79 ± 0.16	120.30 ± 6.95
GravIS + A+O	7.47 ± 0.72	215.09 ± 25.7	2.61 ± 0.72	112.98 ± 98.1
GFZ RL06-SLR_GFZ + A+O	8.75 ± 0.24	220.93 ± 3.78	2.69 ± 0.24	110.50 ± 12.0
GFZ RL06-SLR_TN11 + A+O	7.53 ± 2.35	221.58 ± 4.39	2.76 ± 0.24	112.76 ± 11.4
SLR_TN11 + A+O	8.56 ± 0.24	220.51 ± 3.82	3.03 ± 0.24	107.82 ± 9.71
SLR_Multi	7.09 ± 0.21	233.00 ± 1.72	1.80 ± 0.21	124.32 ± 6.76
SLR_Zhang	7.63 ± ——	218.00 ± ——		
GRACE Average	7.91 ± 0.87	219.30 ± 3.58	2.69 ± 0.10	112.08 ± 1.37
SLR Average	7.71 ± 1.29	223.48 ± 8.03	2.39 ± 0.99	113.96 ± 11.7
Average (GRACE+SLR)	7.80 ± 1.04	221.36 ± 6.12	2.57 ± 0.53	112.78 ± 6.30
YAN	7.15 ± 0.60	230.03 ± 3.00	0.88 ± 0.60	124.45 ± 11.0

Note: The phase is defined as φ in $\sin(\omega(t - t_0) + \varphi)$, where t_0 refers to 0 UTC on January 1 and $\omega = 1/365.25d$.

3.3 Model-based EAM from alternative sources

Alternative model-based EAM time-series for this study were taken from the Global Geophysical Fluids Center (GGFC) of the International Earth Rotation and Reference Systems Service (IERS). AAM from Atmospheric and Environmental Research (AER) based on the Reanalysis-2 of the National Center for Environmental Prediction (NCEP) are available every 6 hr during 1976 and 2017 (Salstein & Rosen 1997). TU Vienna contributed an AAM series (1980–2018, 6 hr) that is also based on ECMWF atmospheric data (Schindelegger *et al.* 2011). The ECCO OAM data set (1993–2017, 6 hr) was calculated by Jet Propulsion Labratory (JPL) using the ocean model ECCO version kf080h (Gross 2009). We note, however, that ECCO does not include any contribution from barystatic sea-level

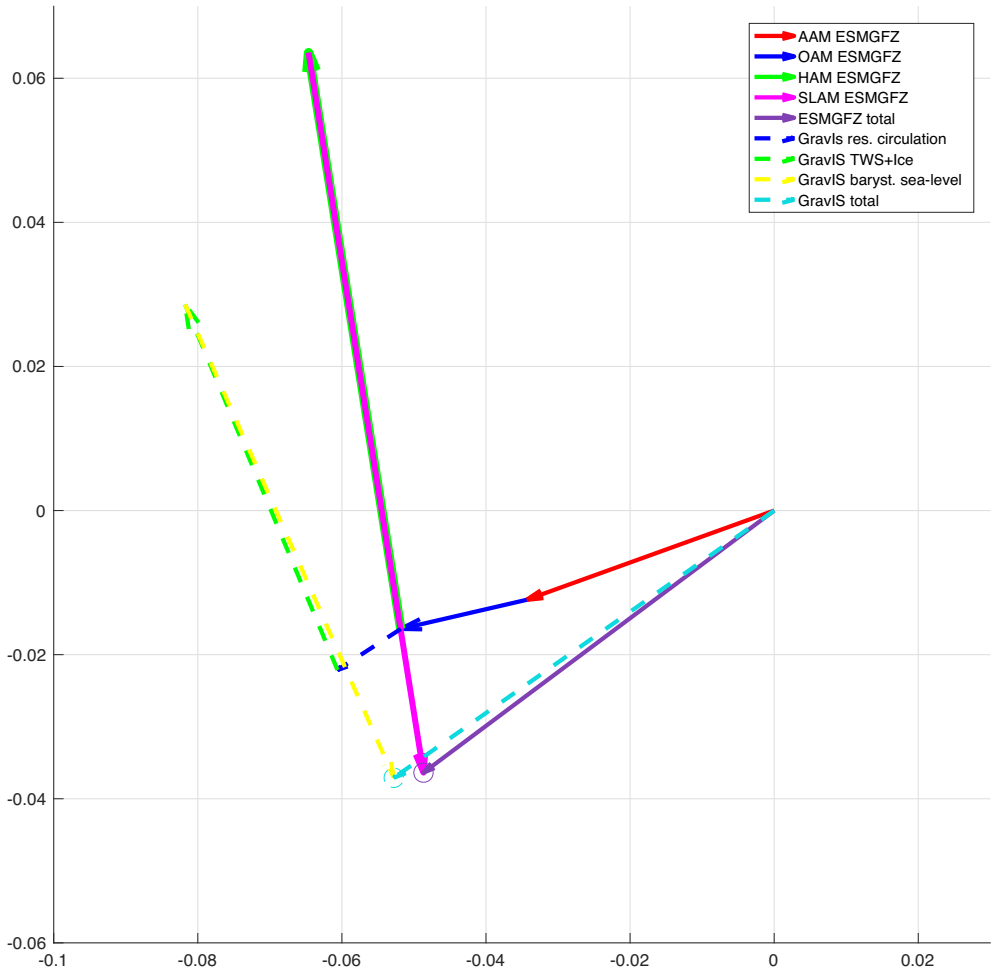

Figure 2. Phasor plot of annual mass term contribution χ_3 mass, part 1. Individual contributions from atmosphere (red), ocean (blue), terrestrial hydrology (green), and barystatic sea level (pink ESMGFZ, yellow GravIS) as well as the sums (purple ESMGFZ, turquoise GravIS) are given for the model ESMGFZ (solid lines) and GRACE L3 product GravIS (dashed lines). Circles represent the uncertainties in estimating the annual harmonic signal. Amplitudes are in milliseconds, phases are defined as φ in $\sin(\omega(t - t_0) + \varphi)$, where t_0 refers to 0 UTC on January 1 and $\omega = 1/365.25d$.

variations, and that no other series exists at the GGFC that covers this process. We therefore rely on seasonal excitation amplitudes and phases based on an a posterior assessment of the global mass budget as published in Yan *et al.* (2012). Those results were calculated from ECMWF atmospheric data, the ECCO ocean synthesis and the GLDAS hydrological model from the years 1980 to 2008.

3.4 GAM from IERS C04

The so-called geodetic angular momentum functions (GAM) are inverted from geodetically observed variations in the Earth's orientation. We utilize the EOP 14 C04 series (Bizouard & Gambis 2008) consistent with the ITRF2014 (Altamimi *et al.* 2016) and calculate EAM from the Liouville equation, eq. (1). Effects of long-period tides were removed from the GAM ΔLOD component as recommended in the IERS conventions (Petit & Luzum 2010,Table 8.1). GAM are available for every day since 1962.

3.5 Mass terms from SLR and GRACE

Mass terms of the total excitation χ_3 are directly related to time-variations of the second degree zonal coefficient ΔC20 of the Earth's gravity field via the MacCullag's formula (see e.g. Chao *et al.* 1988; Chen *et al.* 2012),

$$\chi_3^{\text{mass}} = -\frac{2}{3}\frac{MR^2}{C_m}\Delta C20 \tag{2}$$

where M is the Earth mass, R is the Earth's radius and C_m is the axial moment of inertia of the Earth mantle. SLR is currently the most precise technique to estimate temporal variations of the dynamic flattening of the Earth, and reliable observations extend back as far as 1975, when the Starlette and Lageos satellites were launched. We utilize a time-series of Stokes coefficients from a multisatellite SLR solution (SLR_Multi) as provided by the Center for Space Research (Cheng *et al.* 2011). No geophysical background models were applied in the processing. We further consider the annual amplitudes and phases obtained from a comparable SLR analysis setting reported by Zhang *et al.* (2017) (SLR_Zhang). Third, we use an SLR series that has been specifically calculated to replace ΔC20 in the GRACE RL06 series as published in the GRACE TN11 (SLR_TN11; Cheng *et al.* 2013). Fourth, we test an SLR-series processed at GFZ that considers in total six different satellites (LAGEOS-1 and -2, AJISAI, Stella, Starlette, LARES) but otherwise adheres to the latest GRACE processing standards in the same way as TN11 (SLR_GFZ; König *et al.* 2018). The latter two series

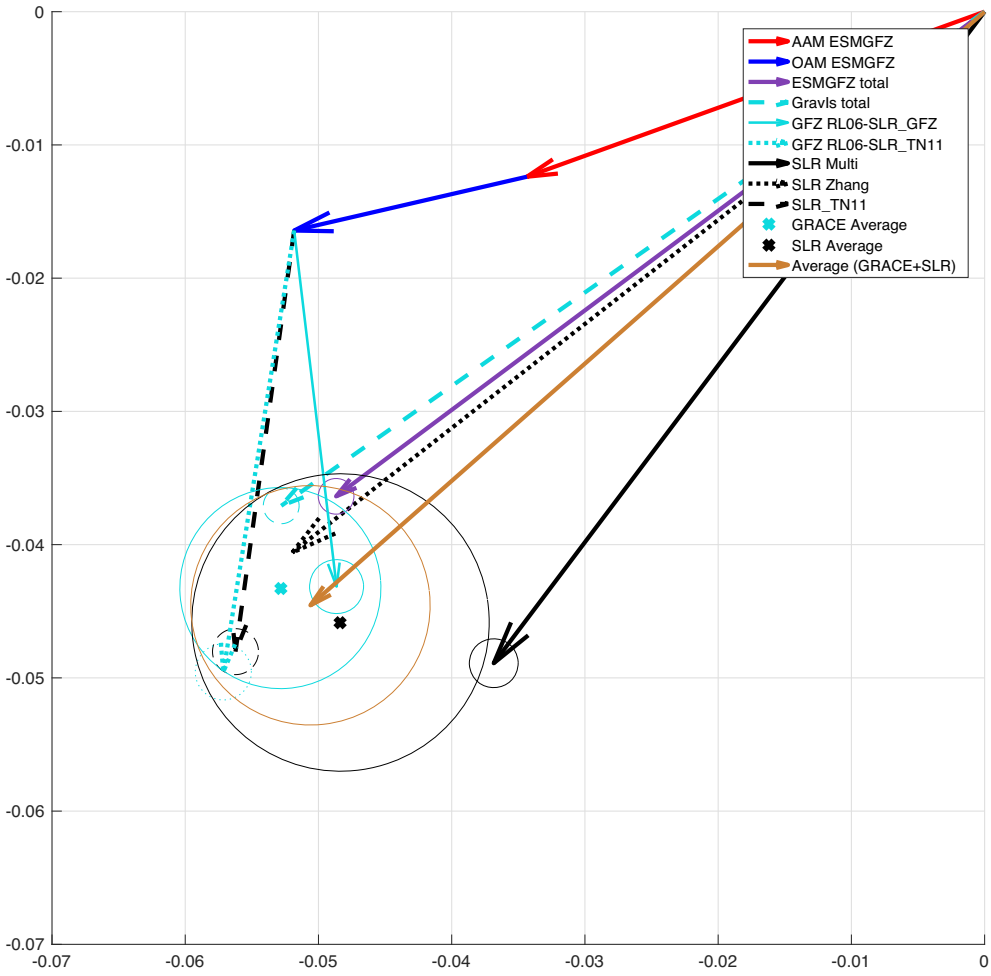

Figure 3. Phasor plot of annual mass term contribution χ_3 mass, part 2. Individual GRACE based estimates (turquoise) for GravIS (dashed), GFZ RL06-SLR_TN11 (dotted) using the $\Delta C20$ replacement SLR_TN11 and GFZ RL06-SLR_GFZ (solid) using SLR_GFZ, like in GravIS. Orange X and circle defines the unweighted average incl. spread of all three GRACE based estimates. Individual SLR estimates (black) based on $\Delta C20$ from a multi-satellite solution (solid), the low degree replacement for GRACE GSM (dashed), and results published by Zhang *et al.* (2017; dotted). Black X and circle defines the unweighted average incl. spread of all three SLR estimates. The average and spread of all satellite (GRACE and SLR) estimates together leads to the mean mass term estimate (brown). For comparison the ESMGFZ model estimate is given in purple. Amplitudes are in milliseconds, phases are defined as φ in $\sin(\omega(t - t_0) + \varphi)$, where t_0 refers to 0 UTC on January 1 and $\omega = 1/365.25d$.

thus utilize the same geophysical background models as applied to GRACE, meaning that non-tidal atmospheric and oceanic effects are reduced via the AOD1B RL06 product.

Satellite gravimetry from GRACE is commonly perceived to be less sensitive to variations in the low-degree Stokes coefficients than SLR and even for the most recent release 06 of the GRACE gravity fields it is still recommended to replace C20 with the values from TN11. However, GRACE has the unique value to provide high-resolution global distributions of seasonal mass variations so that the individual contributions of different regions and dynamic processes can be quantified. We make use of globally gridded monthly mass products based on the GFZ RL06 spherical harmonics solutions as available from the GravIS portal. Available are grids for (i) terrestrial water storage on the continents, (ii) ice mass changes in both Antarctica and Greenland, (iii) barystatic sea-level changes and (iv) ocean bottom pressure variations caused by residual ocean circulation effects not represented in the oceanic background model AOD1B.

The products available from GravIS have been tailored towards anticipated use-cases in hydrology, oceanography or glaciology so that the post-processing and in particular the spatial filtering is different for each individual product. To assess the filtering effects, an alternative GRACE solution has been calculated specifically for this study that shares all processing steps with the GravIS data but applies only the global DDK3 filter. We further note that the GravIS products includes SLR_GFZ, a C20 series calculated at GFZ. To assess the consequences of that processing choice, a second alternative GRACE solution has been calculated that utilizes the SLR_TN11 estimates.

As the GravIS data sets extend so far only until 2016, we restrict all other data sets used in this study to the period 2000 until end of 2016.

4 ANNUAL AND SEMI-ANNUAL MASS TERM VARIABILITY

We initially focus on the effects of the quasi-static mass distribution on the annual and semi-annual harmonic in ΔLOD excitation. We estimated a least squares harmonic fit to the angular momentum

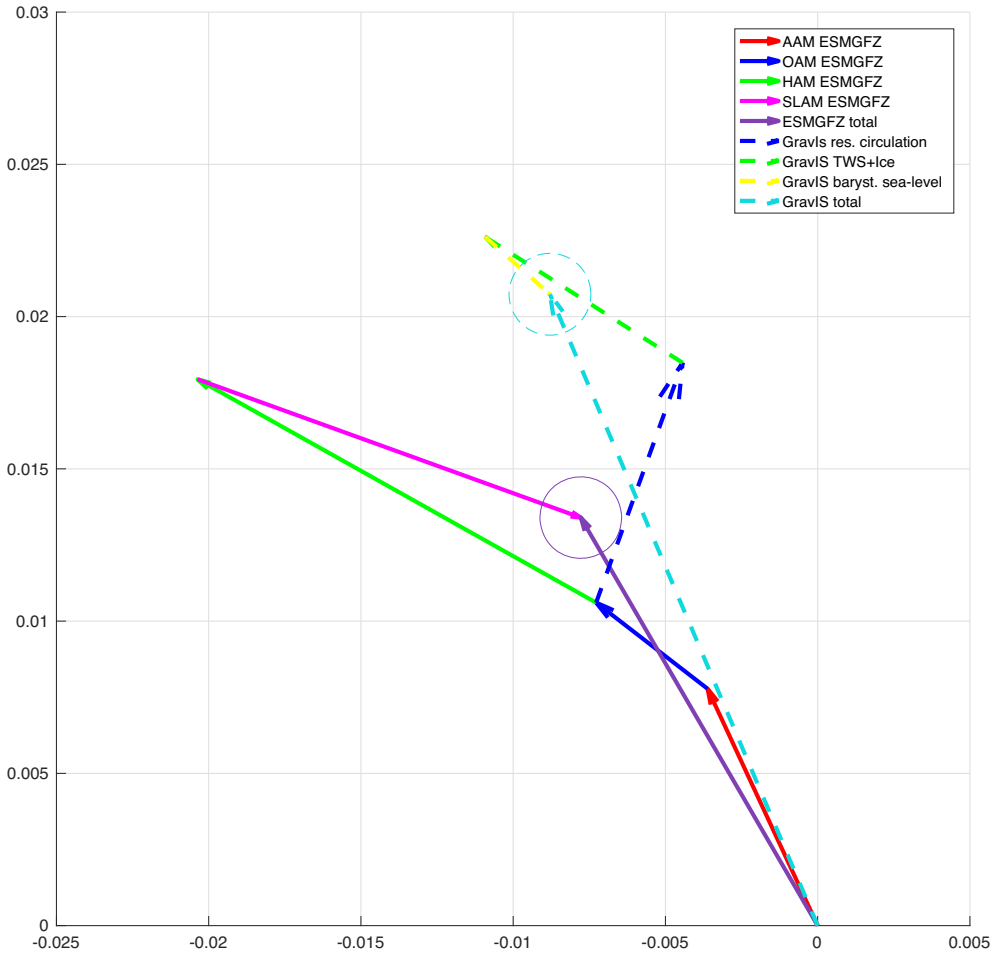

Figure 4. Phasor plot of semi-annual mass term contribution χ_3 mass, part 1. Individual contributions from atmosphere (red), ocean (blue), terrestrial hydrology (green), and barystatic sea level (pink ESMGFZ, yellow GravIS) as well as the sums (purple ESMGFZ, turquoise GravIS) are given for the model ESMGFZ (solid lines) and GRACE L3 product GravIS (dashed lines). Circles represent the uncertainties in estimating the semi-annual harmonic signal. Amplitudes are in milliseconds, phases are defined as φ in $\sin(\omega(t - t_0) + \varphi)$, where t_0 refers to 0 UTC on January 1 and $\omega = 1/365.25d$.

time-series with bias, trend, annual, semi-annual and ter-annual harmonics (Table 1). Although the ter-annual signal reaches in some cases similar amplitudes as the semi-annual signal, this period is not discussed any further. Amplitudes are given in terms of unitless excitation functions, and phases refer to the maximum relative to January 1st. Errors provided solely indicate the determination accuracy of the least squares fit and are thus an indicator for the stability of the seasonal signal over time.

Results are very similar for the atmospheric mass contributions of three different AAM solutions (ESMGFZ, TUV, AER) considered. Estimates for AAM from the GravIS model AOD1B atmosphere differ from the ones obtained from ESMGFZ only due to differences in the temporal sampling (irregular monthly versus regular three hourly). Annual dynamic ocean bottom pressure contributions (i.e. OAM) are well in phase with the atmospheric mass excitations. We note that the annual amplitude of the MPIOM ocean model is much larger than the corresponding result from the ECCO model. Interestingly, residual ocean bottom pressure variability observed by GRACE indicates that MPIOM is still missing a considerable fraction (35 per cent) of the excitation. Based on the internally calculated global DDK3 GRACE solution, we rule out that filtering of the GRACE-based products has not such a great impact on the results. The contribution from GravIS leakage is below 10 per cent in the annual amplitude (0.37×10^{-10}). Thus, filtering and continental leakage only does not explain the difference between ESMGFZ and GravIS OAMs.

HAM from ESMGFZ excite ΔLOD with its maximum amplitude in April almost perpendicular to the effect of atmosphere and oceans peaking in July. The HAM excitation is, however, overcompensated by the SLAM that has almost exactly opposite orientation but a 24 per cent larger magnitude. SLAM arises by 82 per cent from the hydrological balance, 16 per cent from the atmospheric balance and 2 per cent from the gravitational effects of atmospheric and continental water masses on the sea-level topography. Both, magnitude and orientation, of the model-based HAM and SLAM are generally confirmed by the GRACE products available from GravIS. As in the models, TWS effects are again overcompensated by barystatic sea-level excitations. Looking at several GRACE based TWS solutions (not listed here), we found small phase differences of 7–13 d between the individual HAM results that are mainly coming from different coastline representations. Such phase differences are also compensated by the appropriate SLAM contribution. Our results nicely confirm former conclusions by Yan *et al.* (2012) calculated for hydrological data from GLDAS. It clearly indicates that contributions from barystatic sea-level changes or – as it is also called, the global mass balance effect – need to be considered when

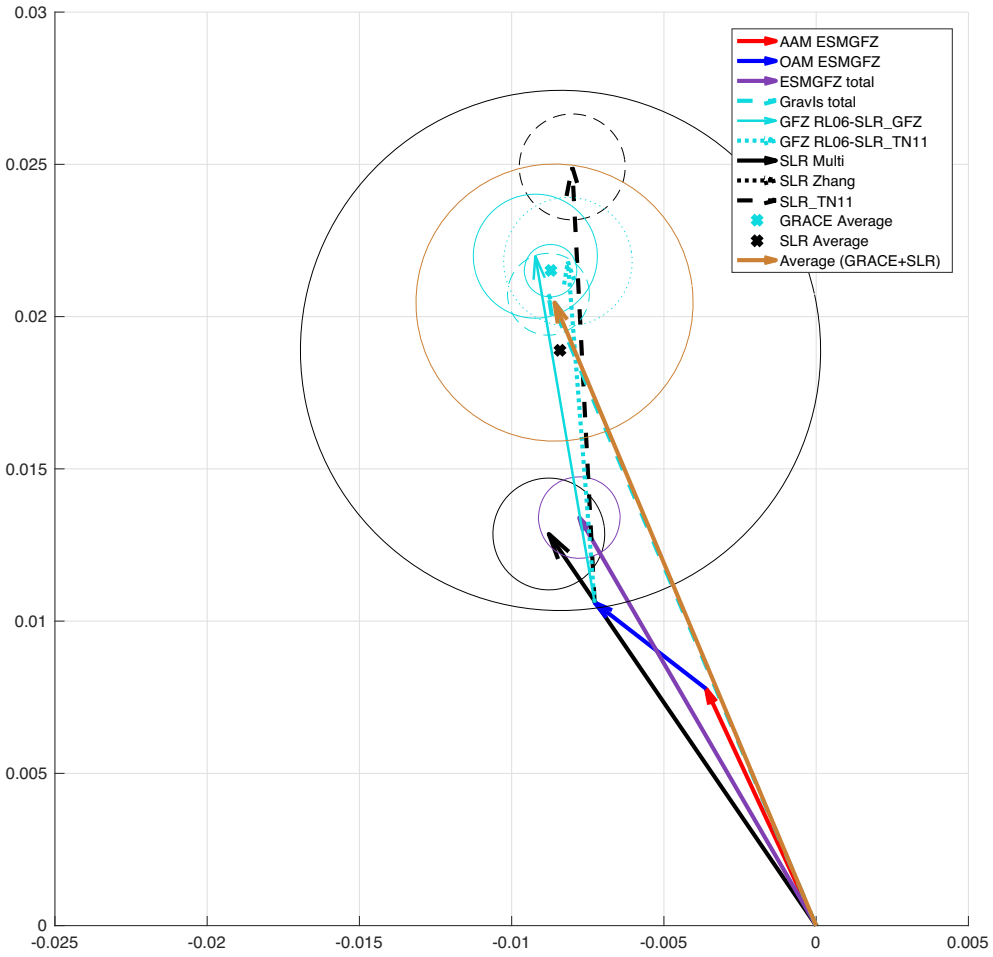

Figure 5. Phasor plot of semi-annual mass term contribution χ_3 mass, part 2. Individual GRACE based estimates (turquoise) for GravIS (dashed), GFZ RL06-SLR_TN11 (dotted) using the $\Delta C20$ replacement SLR_TN11 and GFZ RL06-SLR_GFZ (solid) using SLR_GFZ, like in GravIS. Orange X and circle defines the unweighted average incl. spread of all three GRACE based estimates. Individual SLR estimates (black) based on $\Delta C20$ from a multi-satellite solution (solid), the low degree replacement for GRACE GSM (dashed), and results published by Zhang *et al.* (2017) (dotted). Black X and circle defines the unweighted average incl. spread of all three SLR estimates. The average and spread of all satellite (GRACE and SLR) estimates together leads to the mean mass term estimate (brown). For comparison the ESMGFZ model estimate is given in purple. Amplitudes are in milliseconds, phases are defined as φ in $\sin(\omega(t - t_0) + \varphi)$, where t_0 refers to 0 UTC on January 1 and $\omega = 1/365.25d$.

contributions from different Earth system compartments to annual ΔLOD excitations are being investigated. Different applications of the GMB, for example, global homogeneous distribution like in Yan *et al.* (2012) or solving explicitly the sea-level equation like it is done in GravIS and ESMGFZ, deviate by $\approx$2 per cent in the annual harmonic. Differences are larger for submonthly periods. Summing up all individual mass term contributions, the GravIS and ESMGFZ estimates fit quit well together for the annual signal (Fig. 2). For the semi-annual signal GravIS has a larger amplitude than ESMGFZ (Fig. 4).

The comparison of SLR_TN11 with the GRACE solution GFZ RL06-SLR_TN11 including a replaced C_20 estimate from SLR_TN11 confirms that numerical integration of EAM from global mass grids obtained with GRACE is sufficiently accurate and do not affect the results. In contrast, the choice of an particular SLR solution for the C_20 replacement in the GRACE level 2 processing significantly impacts the results as seen in the differences between GFZ RL06-SLR_TN11 and GFZ RL06-SLR_GFZ. Considering all three GRACE based solutions, the annual mass term is determined with an accuracy of $\pm 0.9 \times 10^{-10}$ in amplitude and $\pm 3.7^\circ$ in phase. We also checked GRACE solutions from other processing centers and found that solutions using the same C_20 replacement (SLR_TN11) lead to almost the identical results for the annual and semi-annual ΔLOD excitation. The other two SLR solutions available to us reveal a somewhat larger deviation from each other with an spread of $\pm 1.3 \times 10^{-10}$ in amplitude and $\pm 8.1^\circ$ in phase. It remains open at this point whether the application of AOD1B as a background contributes to the more robust estimation of C20 from laser tracking data that is highly irregularly distributed both in time and in space. Nevertheless, the unweighted mean of the three SLR solutions leads to almost the same annual mass term signal as the GRACE average estimate. Moreover, the result from the ESMGFZ model fit also quite well within the distribution of all considered geodetic estimates (Figs 3 and 5). We thus conclude that the mass terms of annual ΔLOD excitations is fairly well understood from a combination of satellite gravimetry and numerical models. The semi-annual mass term leads to a well defined estimate from GRACE, SLR estimates have a larger spread and also the model estimate ESMGFZ deviates slightly from the GRACE estimate. Note, that the only monthly resolution of GRACE and also some missing monthly data might influence the semi-annual phase significantly.

5 MONTH-TO-MONTH MASS TERM VARIABILITY

We now extend our assessment to all frequencies captured by monthly mean estimates of time-variations in the Earth's gravity field as observed by satellite gravimetry. We start with showing time-series of 30-d low-pass filtered mass terms from AAM, OAM, HAM, and SLAM as provided by ESMGFZ over the years 2000–2016 (Fig. 6). Ocean and atmospheric mass terms are largely in phase with each other and have about the same magnitudes. HAM and SLAM are much larger than any of the other components, but cancel each other almost perfectly. The latter two series in particular show large inter-annual variations which are believed to be associated with global modes of climate variability as, for example, the El Nino Southern Oscillation (ENSO).

Despite of being based on two different numerical weather predictions models developed in the US and in Europe, the AAM mass terms ESMGFZ relying on ECMWF data and AAM mass from AER obtained from NCEP-2 are remarkably similar (Fig. 7). This is certainly related to the dense coverage of surface pressure gauges in all inhabited regions of the world, and the generally high weight of that data type in the applied data assimilation schemes. The comparison moreover does not indicate any discontinuities or long-term drifts, thereby indicating that the applied mapping to the reference topography has worked well in removing any offsets related to changes in the operational numerical weather prediction model.

When comparing AAM mass terms from ESMGFZ and TUV that both rely on the same atmospheric model (Fig. 8), we note that differences are somewhat smaller than the NCEP residuals, but still not negligible. We suppose that (i) the spatial resolution of the surface pressure data grids, (ii) the representation of the coastline that governs the inverse-barometric correction, and (iii) the chosen reference orography required to account for occasional changes in the operational ECMWF model all contribute to the remaining discrepancies. AAM from TUV do not consider such changes in the ECMWF model, for example, 2007 January 1.

Differences between oceanic mass terms provided by ESMGFZ and JPL are, in contrast, much more different (Fig. 9). ECCO is having generally much smaller amplitudes than MPIOM, and the residuals are frequently as large as the signal from ECCO itself. Reasons for this might reside in the fact that the number of statistically independent observations in the oceans are orders of magnitude smaller than in the atmosphere. Satellite remote sensing usually only provides surface information, and hydrographic information from moorings or autonomous drifters does not sample the oceans in a homogeneous and redundant way. Thus, observations are sometimes averaged over periods from several hours to some days before being assimilated, leading to a diminished variability at subdiurnal to subweekly temporal scales. On the contrary, MPIOM is an unconstrained ocean model run that is only driven by atmospheric matter, energy, and momentum fluxes. Systematic deficits are not at all compensated by data assimilation and thus propagate unchanged into the OAM estimates.

We also look at the residual ocean contribution as seen by GRACE, which consists of (i) the ocean component of the AOD1B a priori model (GravIS model AOD1B ocean), (ii) the residual ocean circulation as provided by GravIS and (iii) the continental leakage of all areas in close proximity to the coasts (Fig. 10). We note that GravIS estimates are consistently larger than the OAM from ESMGFZ, which is identical with the ocean component of AOD1B representing the first summand of the GRACE estimate, though. A few months with particularly high deviations can be traced back to exceptionally short repeat cycles of the GRACE groundtrack pattern (i.e. September 2004), limited thermal control of the sensors (i.e. after the year 2014), a very limited amount of sensor data available within a month due to necessary orbit manoevers and other disruptions of the satellite's normal operations. But even apart from those particular months, the analysis suggests that a substantial amount of ocean variability relevant for ΔLOD exitation is not captured by MPIOM.

The SLAM contributions from ESMGFZ and GravIS correspond very well despite the fact that GravIS includes a substantial trend coming from GIA. According to the slightly overestimated water storage variation in the LSDM model, the modelled SLAM component compensates HAM with higher annual amplitudes than the GRACE estimate. (Fig. 11)

The sum of HAM + SLAM from ESMGFZ can be compared to the space geodetic estimates from GRACE and SLR, both corrected for the model atmosphere and ocean by AOD1B (Fig. 12). Differences in the trend between the GravIS results and SLR-TN11 are due to the GIA effect not corrected from SLR. Apart from the trends, however, seasonal and interannual variability in all three series are highly correlated. We thus conclude that even the month-to-month variability is well understood from a combination of satellite gravimetry and numerical models.

6 SEASONAL MOTION TERM VARIABILITY

On seasonal-to-interannual timescales, the motion term contributions to ΔLOD are clearly dominated by tropospheric winds. OAM current contributions as simulated by MPIOM are almost two magnitudes smaller and river flow effects are entirely negligible (Table 2). AAM motion terms of ESMGFZ, TUV and AER agree very well in their annual phase with residuals being smaller than 2 d. Annual amplitudes of all ECMWF-based estimates are consistent within 0.8 per cent, but lower than NCEP results from AER by about 7 per cent. We also note that the annual amplitude—but not the semi-annual amplitude—of NCEP $\chi_{3,\,motion}$ depends considerably on the analysis period. Whereas ESMGFZ has a rather constant annual amplitude anytime between the years 1980 and 2016, the annual amplitude for NCEP gradually converges from 49.11×10^{-10} (for the years 2000–2016) down to 47.01×10^{-10} (for the years 1990–2000), towards the ECMWF level. This systematic difference certainly reflects different strategies in the data assimilation of upper-air observations into the two different numerical weather prediction models. We note that surface topography resolution does not have a substantial influence on the axial AAM motion term that determines ΔLOD: the difference is less than 1 per cent (see, e.g. Zhou *et al.* 2006).

The annual amplitude and phase of OAM motion is well comparable between ESMGFZ and ECCO (Fig. 13). The semi-annual signal differs substantially in phase, but is at the same time a very small contribution (Fig. 14). The fact that AAM motion terms are two magnitudes larger than the second largest contribution from OAM thus provides an alternative access to AAM $\chi_{3,\,\mathrm{motion}}$ by subtracting the total mass contribution $\chi_{3,\,\mathrm{mass}}$ discussed in the previous section from the geodetically observed excitation of ΔLOD.

We therefore calculate two variants of pseudo-observed $\chi_{3,\,\mathrm{motion}}$ terms: (i) by using $\chi_{3,\,\mathrm{mass}}$ terms from the sum of AAM, OAM, HAM and SLAM from ESMGFZ; and (ii) by using the unweighted average of all GRACE and SLR estimates discussed above. With respect to the different amplitudes of the total mass and the total

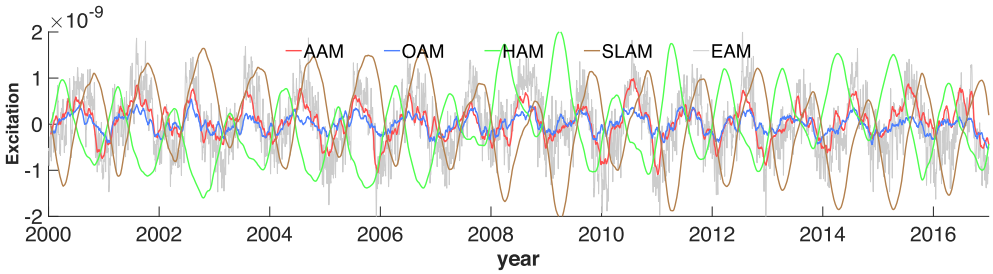

Figure 6. Monthly signal in ESMGFZ χ_3 mass terms. Time-series of AAM (red), OAM (blue), HAM (green), SLAM (brown), filtered with 30-d moving average. Total EAM (grey) daily values.

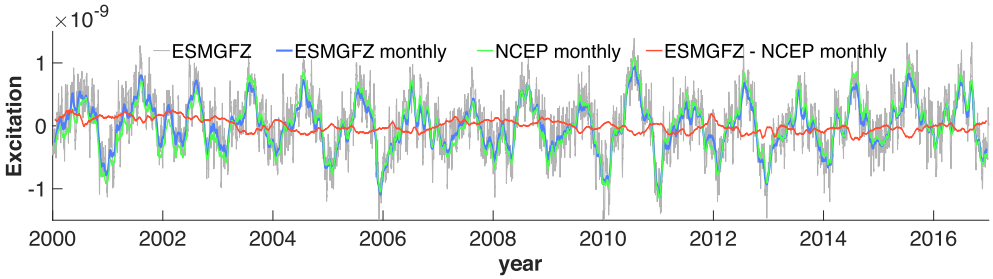

Figure 7. AAM contribution to χ_3 mass. ESMGFZ daily (grey), ESMGFZ monthly (blue), NCEP monthly (green), difference ESMGFZ − NCEP (red).

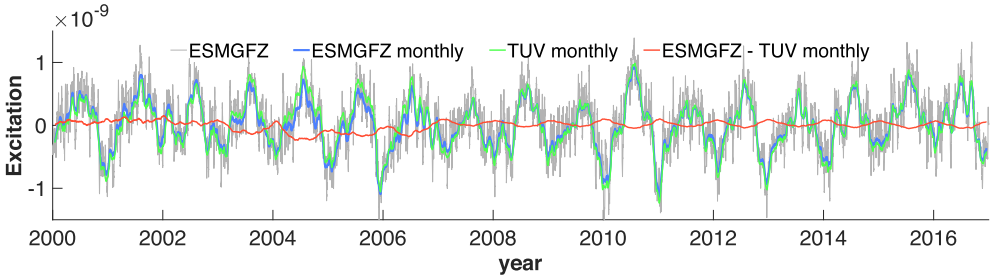

Figure 8. AAM contribution to χ_3 mass. ESMGFZ daily (grey), ESMGFZ monthly (blue), TUV monthly (green), difference ESMGFZ − TUV (red).

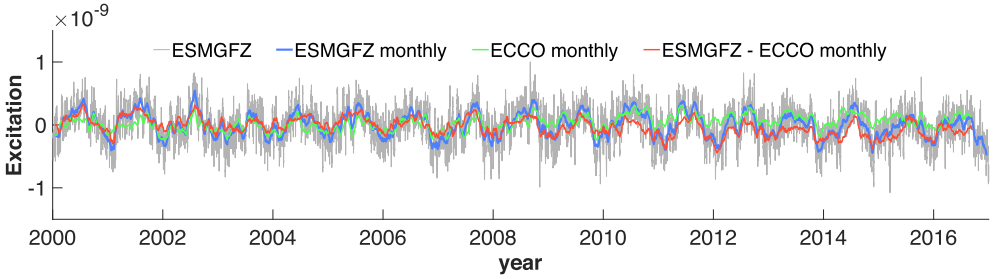

Figure 9. OAM contribution to χ_3 mass. ESMGFZ daily (grey), ESMGFZ monthly (blue), ECCO monthly (green), difference ESMGFZ − ECCO (red).

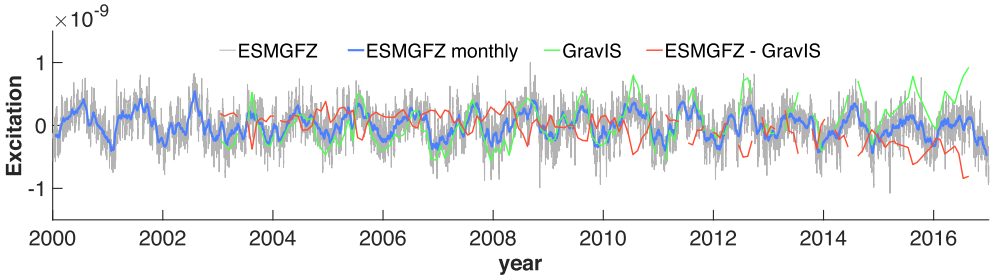

Figure 10. OAM contribution to χ_3 mass. ESMGFZ daily (grey), ESMGFZ monthly (blue), GravIS model AOD1B ocean + residual circulation + leakage (green), difference ESMGFZ − GravIS (red).

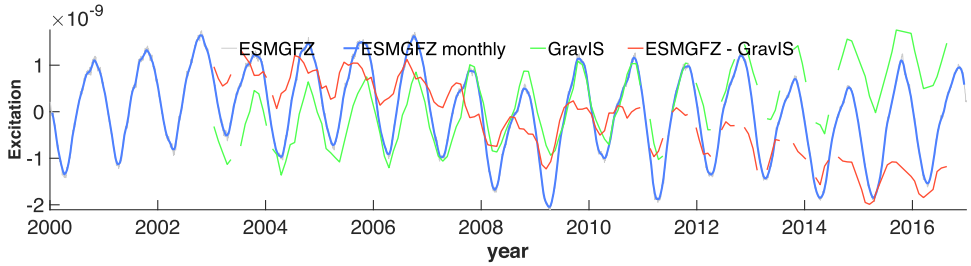

Figure 11. SLAM contribution to χ_3 mass. ESMGFZ daily (grey), ESMGFZ monthly (blue), GravIS barystatic sea level (green), difference ESMGFZ − GravIS (red).

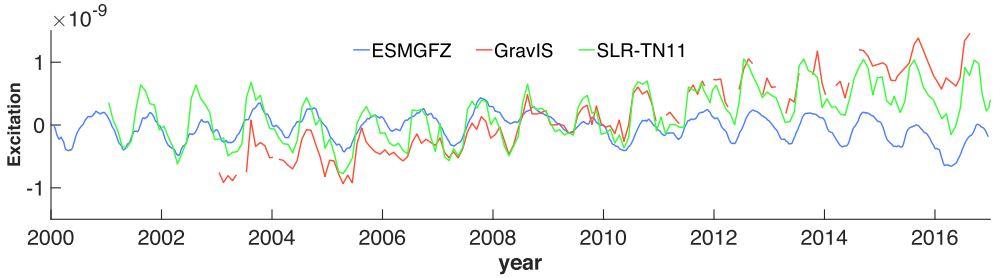

Figure 12. Total excitation in χ_3 mass reduced by ESMGFZ model atmosphere and ocean. ESMGFZ (blue), GravIS (red), SLR_TN11 (green).

Table 2. Seasonal signal in χ_3 motion term

	Annual		Semi-annual	
	Amplitude (10^{-10})	Phase (deg)	Amplitude (10^{-10})	Phase (deg)
AAM motion				
ESMGFZ (ECMWF)	45.81 ± 0.14	34.43 ± 0.17	30.34 ± 0.14	252.51 ± 0.26
TUV (ECMWF)	46.61 ± 0.20	34.09 ± 0.24	30.48 ± 0.20	253.75 ± 0.37
AER (NCEP)	49.11 ± 0.19	33.13 ± 0.23	25.81 ± 0.19	254.47 ± 0.43
YAN (ECMWF)	46.47 ± 0.32	34.00 ± 0.00	30.60 ± 0.32	41.00 ± 1.00
OAM motion				
ESMGFZ (MPIOM)	0.68 ± 0.01	171.86 ± 1.21	0.14 ± 0.01	294.86 ± 5.89
JPL (ECCO)	0.88 ± 0.03	189.17 ± 1.87	0.22 ± 0.03	217.59 ± 7.56
YAN (ECCO)	0.87 ± 0.01	205.00 ± 1.00	0.20 ± 0.01	123.00 ± 2.00
AAM motion + OAM motion				
ESMGFZ	45.31 ± 0.15	35.01 ± 1.51	30.46 ± 0.15	252.65 ± 6.15
NCEP + ECCO	48.30 ± 0.22	33.56 ± 2.09	25.98 ± 0.22	254.18 ± 7.99
Average motion	46.80 ± 2.27	34.26 ± 1.03	28.22 ± 3.21	253.35 ± 1.08
YAN	45.61 ± 0.33	34.17 ± 2.00	30.63 ± 0.33	41.37 ± 3.00
AAM motion (+7%) + OAM motion				
ESMGFZ+7	48.52 ± 0.16	34.96 ± 0.38	32.58 ± 0.16	252.64 ± 6.15
AAM motion (+8%) + OAM motion				
ESMGFZ+8	48.98 ± 0.16	34.97 ± 1.38	32.88 ± 0.16	252.64 ± 6.15
GAM - mass				
GAM - ESMGFZ	48.74 ± 0.66	35.01 ± 2.05	31.88 ± 0.66	251.25 ± 7.89
GAM - GRACE Average	49.58 ± 1.37	35.46 ± 4.27	32.75 ± 0.61	251.96 ± 2.31
GAM - SLR Average	49.33 ± 1.79	36.10 ± 8.73	32.47 ± 1.49	251.73 ± 12.6
GAM - Average mass	49.45 ± 1.54	35.78 ± 6.81	32.64 ± 1.03	251.87 ± 7.24
GAM - YAN	48.62 ± 1.10	36.96 ± 3.69	31.25 ± 1.10	250.07 ± 11.9

Note: The phase is defined as φ in $\sin(\omega(t - t_0) + \varphi)$, where t_0 refers to 0 UTC on January 1 and $\omega = 1/365.25d$.

motion terms, the uncertainties arising from the differences of those two mass term estimates account only for 2 per cent for both the annual and semi-annual amplitude of the $\chi_{3,\,\mathrm{motion}}$ terms. There is almost no contribution of the mass term to the phase uncertainty. Hence, the match between pseudo-observed and modelled $\chi_{3,\,\mathrm{motion}}$ terms represents to a large extent the ability of the numerical weather models to capture the seasonal wind variations. By introducing a scaling factor that linearly increases the ECMWF wind terms by +7 per cent we would be able to obtain a remarkable closure of the IERS C04 ΔLOD excitation budget for the ESMGFZ mass term combination. The remaining difference between pseudo-observed and modelled $\chi_{3,\,motion}$ term is only 0.4 per cent in the annual and 0.1 per cent in the semi-annual amplitude.

When using the mass term estimates from GRACE/SLR, the ECMWF wind terms appear to be underestimated by even 8 per cent or more, and also the NCEP wind terms are some 2 per cent too low. Previous studies Chao & Yan (2010) suggested that the atmospheric circulation models in general underestimate AAM wind terms by

Table 3. List of acronyms.

AAM	Atmospheric angular momentum function
AER	Atmospheric and Environmental Research Center
AOD1B	Atmosphere and ocean non-tidal de-aliasing product
CPC	Climate Prediction Center at NOAA, USA
DDK	Decorrelation and non-isotropic smoothing filter
ΔLOD	Change in length-of-day
ECMWF	European Centre for Medium-range Forecast
EAM	Effective angular momentum function (AAM, OAM, HAM, SLAM)
ECCO	Estimating the circulation and climate of the ocean—ocean model
ENSO	El Niño and Southern Oscillation
ESMGFZ	Earth System Modelling group at GFZ Potsdam
GAM	Geodetic angular momentum
GFZ	Helmholtz Centre Potsdam GFZ German Research Centre for Geosciences
GGFC	IERS Global Geophysical Fluids Centre
GLDAS	Global Land Data Assimilation System, NASA—hydrological model
GMB	Global mass balance
GRACE	Gravity Recovery And Climate Experiment—satellite mission
GravIS	GFZ—Gravity Information Service
HAM	Hydrological angular momentum
IERS	International Earth Rotation and Reference Systems Service
JPL	NASA Jet Propulsion Laboratory
LSDM	Land Surface Discharge Model—hydrological model
MPIOM	Max Planck Institute Ocean Model—ocean model
NCEP	National Centers for Environmental Prediction at NOAA, USA
OAM	Oceanic angular momentum
SLAM	Sealevel angular momentum
SLR	Satellite laser ranging
TN11	GRACE Technical Note 11 (monthly estimates of C20 from SLR)
TUV	Technical University Vienna
VDK	Time-variable decorrelation and non-isotropic smoothing filter

10 per cent-20 per cent on intraseasonal-to-seasonal timescales and Yan *et al.* (2012) found a possible underestimation of ≈7 per cent in the ECMWF wind terms of that time. The change in annual AAM motion term amplitudes in NCEP from over the decades indicates that those parts of the atmospheric circulation primarily responsible for LOD excitation are not yet tightly constrained by observations. Therefore, we argue that a 7–8 per cent underestimation as indicated by the pseudo-observed AAM motion terms is not entirely unrealistic and thus ask for a renewed scrutiny in the assessment of upper-air wind fields primarily responsible for Earth orientation changes.

7 MONTH-TO-MONTH MOTION TERM VARIABILITY

We finally extend also the assessment of motion term variability to all frequencies captured by monthly mean estimates. When comparing time-series from ESMGFZ and TUV (Fig. 15), both time-series are almost perfectly aligned to each other. Deviations are larger between ESMGFZ and AER (Fig. 16), with a tendency of AER to somewhat underestimate the extreme values in the excitation, which might be related to the lower horizontal and vertical resolution of the NCEP data-set employed here. Motion terms from OAM of ESMGFZ and JPL differ from each other to a large extent (Fig. 17), but are also at timescales considered here much smaller than the atmospheric wind effects.

We finally look at the residuals of the EAM combinations with respect to the geodetically observed GAM (Fig. 18). The residual motion term of the modelled ESMGFZ time-series and pseudo-observation GAM reduced by the ESMGFZ mass terms shows no apparent systematic. The month-to-month variability only improves slightly when increasing the AAM wind terms by 7 per cent. In addition to the results for the semi-annual term, this is another indication that the systematic underestimation of 7 per cent of the wind component is dominant only in the annual term.

8 DISCUSSION

In order to validate the atmospheric motion excitation as calculated from predicted winds of numerical weather models against geodetic observation of Earth rotation, we first assess all other contributions coming from mass redistributions within the Earth system components atmosphere, ocean, and continental hydrosphere. Especially, the interactions between this subsystems via the global hydrological cycle cause substantial mass redistributions among atmosphere, ocean and continents that cannot be ignored when analysing the seasonal cycle in ΔLOD excitation. Estimates of the seasonal signal amplitudes and phases of ESMGFZ SLAM comprising the influence of global mass conservation confirm former studies on the GMB effect, that the consideration of the full hydrological influence, HAM+SLAM, is essential for reasonable results of the total mass induced signal in annual ΔLOD excitation. SLAM overcompensates the HAM contribution with a 24 per cent higher annual amplitude and an opposite phase, shifted by 6 month. Although individual HAM components from different models or GRACE solutions vary significantly in amplitude and partly in phase, the balanced hydrological excitation HAM+SLAM become highly comparable. Adding also the atmospheric mass balance, that compensates about half of the AAM mass term, the differences further decrease. When combining various individual excitation sources, one has to be aware, that the GMB effect corresponds to the specific choice of the underlying atmospheric and hydrological model

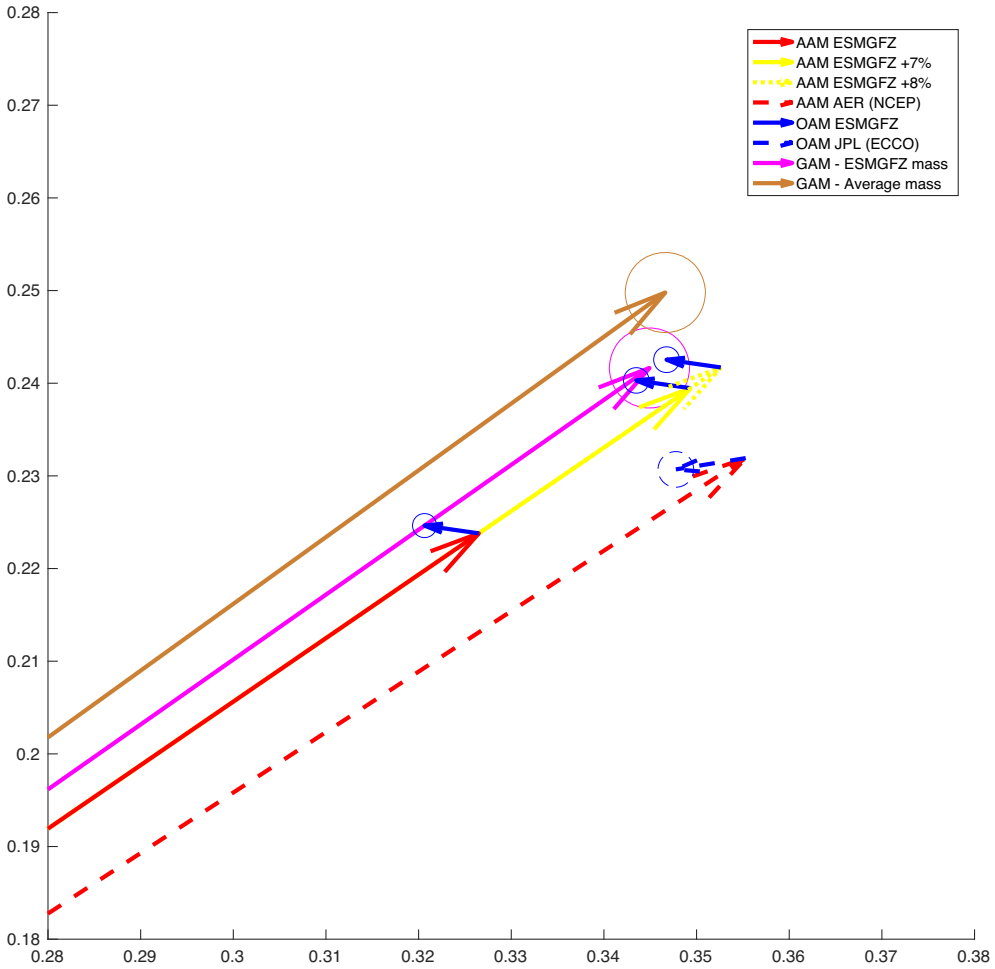

Figure 13. Phasor plot of annual motion term contribution χ_3 motion. Contributions of atmospheric winds (red) from ESMGFZ ECMWF (solid) and AER NCEP (dashed). Contributions of ocean currents (blue) from ESMGFZ MPIOM (solid) and JPL ECCO (dashed). Contributions of enhanced atmospheric winds (yellow) from ESMGFZ ECMWF + 7 per cent (solid) and from ESMGFZ ECMWF + 8 per cent (dotted). Pseudo-observation using GAM (IERS C04) reduced by the ESMGFZ mass term (purple) and the average mass term from GRACE/SLR satellite solutions (brown). Amplitudes are in milliseconds, phases are defined as φ in $\sin(\omega(t - t_0) + \varphi)$, where t_0 refers to 0 UTC on January 1 and $\omega = 1/365.25d$. Circles represent the uncertainties in estimating the annual harmonic signal.

and is therefore uniquely applicable only for one chosen model combination.

Alternatively to the sum off all mass induced geophysical fluid excitation functions, we used estimates of the ΔLOD mass term derived from satellite missions GRACE and SLR. It turns out, that GRACE based solution are highly comparable between different processing centres but are very sensitive to the applied ΔC20 replacement derived from two different SLR solutions. This considerable diversity in SLR ΔC20 estimates is further supported by three more SLR solutions considered in this study. Nevertheless, the mass terms can be determined accurate enough from the ESMGFZ model combination as well as from an average of all satellite based ΔC20 solutions to attribute the mismatch between modelled and observed seasonal ΔLOD excitation clearly to the modelled motion terms. As the OAM motion due to ocean currents is much smaller than the AAM motion term due to atmospheric winds, we recommend a renewed scrutiny in the assessment of upper-air wind fields. Especially ECMWF tends to underestimate strong atmospheric winds by -7 per cent. After magnification of the ECMWF wind terms by 7 per cent the excitation budget of all ESMGFZ terms perfectly matches the geodetic observation. Using the unweighted mean of all GRACE and SLR ΔC20 solutions as mass term, the ECMWF wind terms seem to be underestimated by even 8 per cent. Looking at the monthly variability, the amplitude of the ECMWF wind terms seem to be much closer the geodetic pseudo-observation.

The conclusion of underestimated atmospheric winds is also supported by several studies comparing upper air wind predictions from numerical weather models with commercial aviation data. Modelled wind speeds above 20 m s^{-1} reveal a remarkably constant bias of -4 per cent to -6 per cent where the high-resolution models have always less bias than the lower-resolution models (Rickard *et al.* 2001). Applying a constant multiplier (presently set at 1.04) to the wind speeds forecasted by the Met Office the flight time errors are best minimized. Likely, assimilation systems used at the major weather operational centres (e.g. ECMWF, NCEP) tend to smooth sharp gradients, especially near the strong jets, resulting in too weak jet streaks by −5 per cent to −9 per cent (Cardinali *et al.* 2004). Jet streams are the predominant source of wind-induced seasonal ΔLOD variations. The AAM motion term might also be underestimated due to errors in simulating the position of subtropical jets during the northern hemisphere winter (Zhou *et al.* 2006).

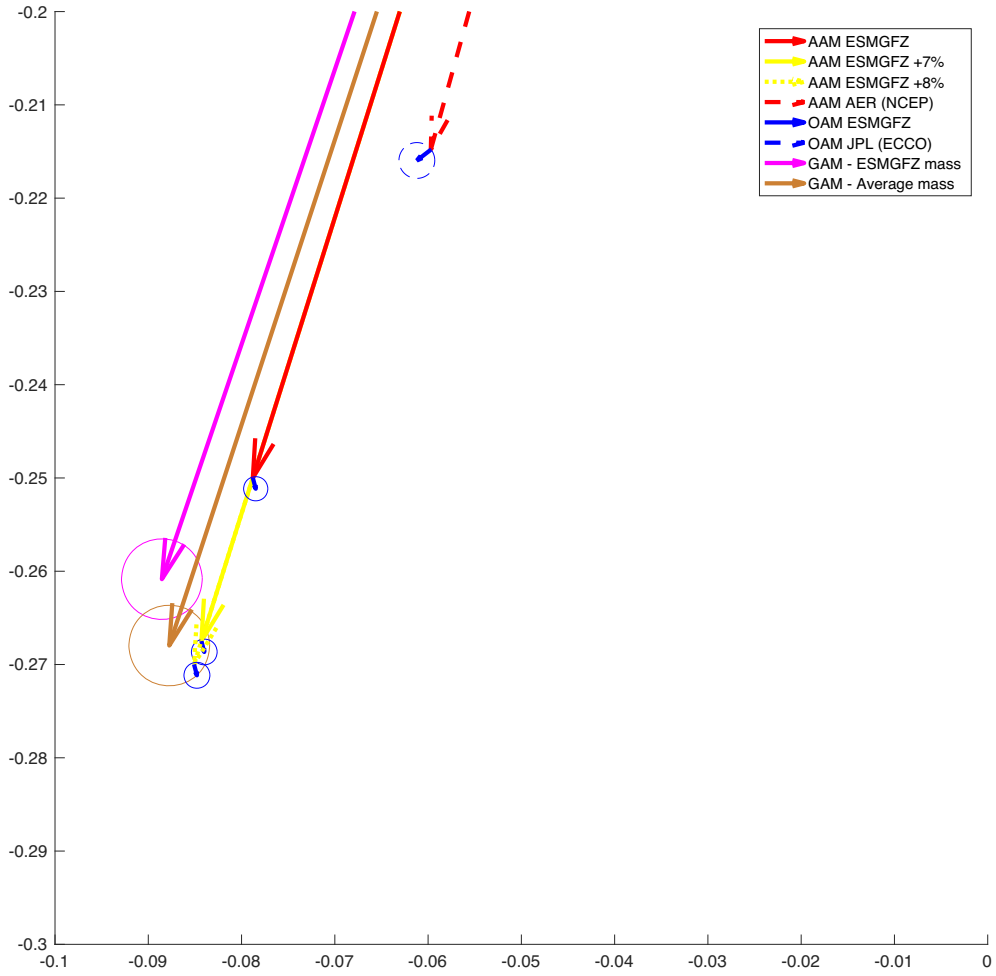

Figure 14. Phasor plot of semi-annual motion term contribution χ_3 motion. Contributions of atmospheric winds (red) from ESMGFZ ECMWF (solid) and AER NCEP (dashed). Contributions of ocean currents (blue) from ESMGFZ MPIOM (solid) and JPL ECCO (dashed). Contributions of enhanced atmospheric winds (yellow) from ESMGFZ ECMWF + 7 per cent (solid) and from ESMGFZ ECMWF + 8 per cent (dotted). Pseudo-observation using GAM (IERS C04) reduced by the ESMGFZ mass term (purple) and the average mass term from GRACE/SLR satellite solutions (brown). Amplitudes are in milliseconds, phases are defined as φ in $\sin(\omega(t - t_0) + \varphi)$, where t_0 refers to 0 UTC on January 1 and $\omega = 1/365.25d$. Circles represent the uncertainties in estimating the semi-annual harmonic signal.

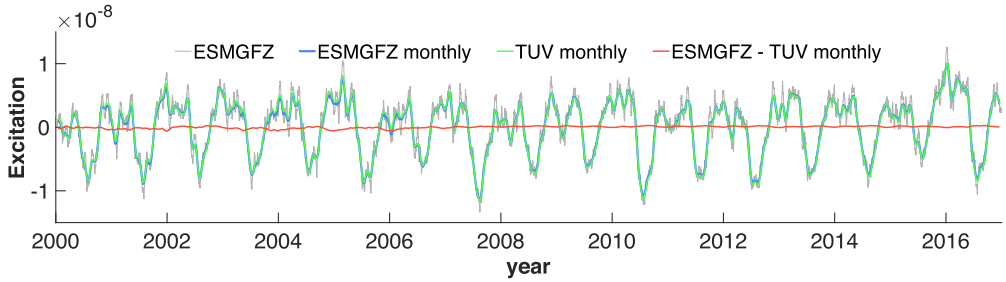

Figure 15. AAM contribution to χ_3 motion. ESMGFZ daily (grey), ESMGFZ monthly (blue), TUV monthly (green), difference ESMGFZ − TUV (red).

The comparison of GRACE-based estimates of the ocean circulation induced OAM mass signal with the AOD1B ocean mass signal based on MPIOM simulations reveals ocean circulation contributions observed by GRACE and SLR not covered from the MPIOM model. Possible error sources like filtering and signal separation seem to be too low to explain the differences. The oceanic contributions seems to be more sensitive to the selected epoch than all other contributions from atmosphere and hydrology, the annual mass term amplitude changes by 1 per cent, its phase by 2 per cent. The annual OAM motion amplitude is even more sensitive to the selected epoch with changes in the range of 12 per cent, phase by 22 per cent. Although, the shorter time span of the GRACE data sets starting in 2002 and the significantly higher determination errors of the seasonal harmonics from the monthly GRACE solutions influence the GRACE based mass term determination the reason for discrepancy between MPIOM modelled ocean circulation and the GRACE/SLR observation needs still more attention.

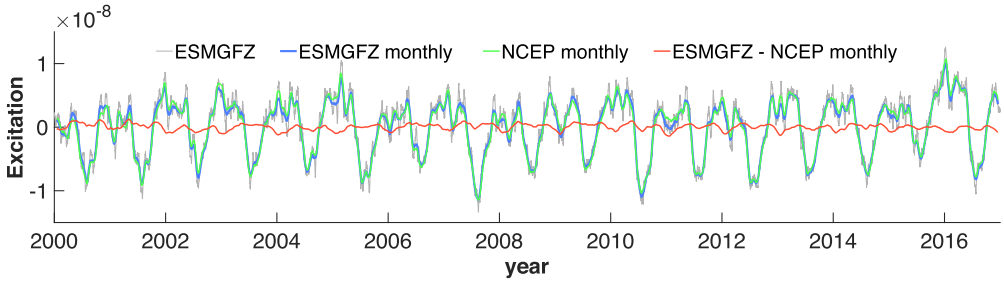

Figure 16. AAM contribution to χ_3 motion. ESMGFZ daily (grey), ESMGFZ monthly (blue), NCEP monthly (green), difference ESMGFZ − NCEP (red).

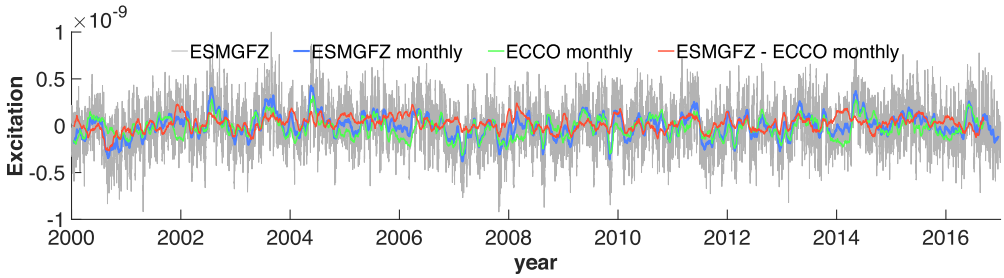

Figure 17. OAM contribution to χ_3 motion. ESMGFZ daily (grey), ESMGFZ monthly (blue), ECCO monthly (green), difference ESMGFZ − ECCO (red).

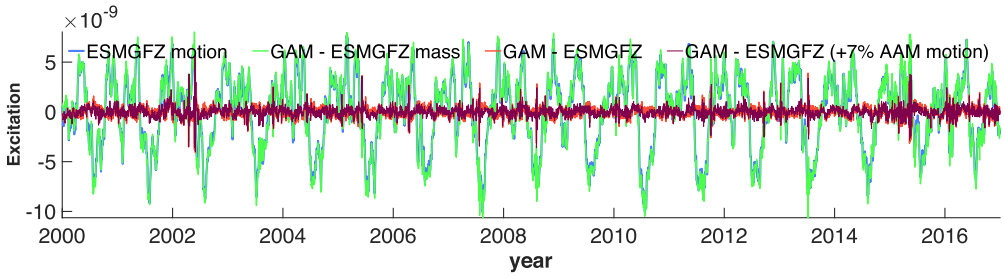

Figure 18. Total excitation in χ_3 motion. ESMGFZ motion term from atmospheric winds and oceanic currents (blue), Pseudo-observed motion term from GAM − ESMGFZ mass term (green) and the difference GAM − ESMGFZ (red). Same difference with ESMGFZ AAM motion term increased by 7 per cent (purple).

In addition to the global mass conservation, we ensured also gravitational consistency by solving explicitly the sea-level equation. Changes in the gravity field and surface deformation due to non-uniform surface mass variations induce the so-called self-attraction and loading effects that change the SLAM excitation of annual ΔLOD by 2 per cent. The equatorial EAM functions χ_1 and χ_2 exciting polar motion seem to be affected much more by the non-uniform changes in ocean bottom pressure. So far, there are only a few studies of low-degree gravity harmonics including self-attraction and loading effects (e.g. Clarke *et al.* 2005; Quinn *et al.* 2015). Although the influence on annual degree-2 harmonics is much smaller than the GMB itself, the local sea level might be significantly different at tide gauges or in-situ bottom pressure observations.

9 SUMMARY

The seasonal variations in length of day are mainly excited by atmospheric wind changes and second by mass redistributions within and among the Earth system components atmosphere, ocean, and continental hydrosphere. With the ESMGFZ SLAM product, considering the influence of global mass conservation, GFZ provides for the first time a consistent set of all Earth rotation angular momentum functions (AAM, OAM, HAM and SLAM) routinely as regularly updated time-series. SLAM is the most important seasonal contribution to ΔLOD after the atmospheric winds. Summing up all mass term contributions, the ESMGFZ model combination as well as comparable estimates from GRACE and SLR satellite missions are able to define the total mass term with an accuracy of ±1.0 × 10^{-10} in amplitude and ±4.0° in phase. Subtracting the mass term contribution from the geodetically observed excitations, the mismatch between modelled and observed seasonal ΔLOD excitation can be attributed to the modelled motion terms. Intensifying the ECMWF wind terms by 7 per cent the excitation budget of modelled ESMGFZ perfectly represents the geodetic ΔLOD observation.

ACKNOWLEDGEMENTS

Deutscher Wetterdienst, Offenbach, Germany, and the European Centre for Medium-Range Weather Forecasts, ECMWF, are acknowledged for providing atmospheric data from their operational odels. Numerical simulations were performed at Deutsches Klimarechenzentrum, DKRZ, in Hamburg, Germany. Data from the Gravity Information Service, GravIS, data can be obtained from http://gravis.gfz-potsdam.de. Effective angular momentum data, EAM, from the Earth System Modelling group at GeoForschungsZentrum, ESMGFZ, in Potsdam is available at http://esmdata.gfz-potsdam.de:8080.

REFERENCES

Altamimi, Z., Rebischung, P., Metivier, L. & Collilieux, X., 2016. ITRF2014: a new release of the International Terrestrial Reference Frame modeling nonlinear station motions, *J. geophys. Res.,* **121,** doi:10.1002/2016JB013098.

Barnes, R.T.H., Hide, A., White, A. & Wilson, C.A., 1983. Atmospheric angular-momentum fluctuations, length-of-day changes and polar motion, *Proc. R. Soc. A,* **387**(1792), 31–73.

Bizouard, C. & Gambis, D., 2008. The combined solution C04 for Earth orientation parameters, recent improvements, in *Series on International Association of Geodesy Symposia,* Vol. **134,** p. 330, ed. Drewes, H., Springer.

Brzezinski, A., Nastuala, J. & Kolaczek, B., 2009. Seasonal excitation of polar motion estimated from recent geophysical models and observations, *J. Geodyn.,* **48,** 235–240.

Brzezinski, A., 1992. Polar motion excitation by variations of the effective angular momentum function: considerations concerning deconvolution problem, *Manuscr. Geod.,* **17,** 3–20.

Cardinali, C., Rukhovets, L. & Tenenbaum, J., 2004. Jet stream analysis and forecast errors using aircraft observations in the DAO, ECMWF, and NCEP models, *Mon. Weather Rev.,* **132,** 764–779.

Chao, B.F. & O'Connor, W.P., 1988. Effect of a uniform sea-level change on the Earth's rotation and gravitational field, *Geophys. J. Int.,* **93,** 191–193.

Chao, B.F. & Yan, H., 2010. Relation between length-of-day variation and angular momentum of geophysical fluids, *J. geophys. Res.,* **115,** B10417, doi:10.1029/2009JB007024

Chen, J.L. & Wilson, C.R., 2005. Hydrological excitations of polar motion, 1993-2002, *Geophys. J Int.,* **160,** 833–839.

Chen, J., 2005. Global mass balance and the length-of-day variation, *J. geophys. Res.,* **110,** B08404, doi:10.1029/2004JB003474.

Chen, J.L., Wilson, C.R. & Zhou, Y.H., 2012. Seasonal excitation of polar motion, *J. Geodyn.,* **62,** 8–15.

Cheng, M.K., Tapley, B.D. & Ries, J.C., 2013. Deceleration in the Earth's oblateness, *J. geophys. Res.,* **118,** 1–8.

Cheng, M., Ries, J.C. & Tapley, B.D., 2011. Variations of the Earth's figure axis from satellite laser ranging and GRACE, *J. geophys. Res.,* **116,** B01409, doi:10.1029/2010JB000850.

Clarke, P.J., Lavallée, D.A., Blewitt, G., van Dam, T.M. & Wahr, J.M., 2005. Effect of gravitational consistency and mass conservation on seasonal surface mass loading models, *Geophys. Res. Lett.,* **32,** L08306, doi:10.1029/2005GL022441.

Dahle, C., Flechtner, F., Gruber, Ch., König, D., König, R., Michalak, G. & Neumayer , K.-H., , 2018. GRACE 327-743 (Gravity Recovery and Climate Experiment): GFZ Level-2 Processing Standards Document for Level-2 Product Release 06 (Rev. 1.0, October 26, 2018), Scientific Technical Report STR - Data; 18/04, p. 20, GFZ German Research Centre for Geosciences, Potsdam, doi:10.2312/GFZ.b103-18048.

Dill, R., 2008. Hydrological model LSDM for operational Earth rotation and gravity field variations, Scientific Technical Report STR; 08/09, p. 35, GFZ Potsdam, Germany.

Dobslaw, H., Dill, R., Grötzsch, A., Brzezinski, A. & Thomas, M., 2010. Seasonal polar motion excitation from numerical models of atmosphere, ocean, and continental hydrosphere, *J. geophys. Res.,* **115**(B10), 406, doi:10.1029/2009JB007127.

Dobslaw, H., 2016. Homogenizing surface pressure time-series from operational numerical weather prediction models for geodetic applications, *J. Geod. Sci.,* **6,** 61–68.

Dobslaw, H. & Dill, R., 2017. Predicting Earth rotation variations from global forecasts of atmosphere-hydrosphere dynamics, *Adv. Space Res.,* doi:10.1016/j.asr.2017.11.044.

Greatbatch, R.J., 1994. A note on the representation of steric sea level in models that conserve volume rather than mass, *J. geophys. Res.,* **99,** 12 767–12 771.

Gross, R.S., 2009. An improved empirical model for the effect of long-period ocean tides on polar motion, *J. Geod.,* **83**(7), 635–644.

Gross, R.S., Fukumori, I., Menemenlis, D. & Gegout, P., 2004. Atmospheric and oceanic excitation of length-of-day variations during 1980-2000, *J. geophys. Res.,* **109,** B01406, doi:10.1029/2003JB002432.

Hagemann, S. & Dümenil, L., 1998. A parametrization of the lateral waterflow for the global scale, *Clim. Dyn.,* **14,** 17–31.

Hagemann, S. & Dümenil, L., 1998. Documentation for the Hydrological Discharge Model, Technical Report, No. 17, Max Planck Institute for Meteorology, Hamburg, Germany.

Hagemann, S. & Dümenil Gates, L., 2003. Improving a subgrid runoff parameterization scheme for climate models by the use of high resolution data derived from satellite observations, *Clim. Dyn.,* **21,** 349–359.

Jungclaus, J.H., Fischer, N., Haak, H., Lohmann, K., Marotzke, J., Matei, D., Mikolajewicz, U., Notz, D. & von Storch, J.S., 2013. Characteristics of the ocean simulations in the Max Planck Institute Ocean Model (MPIOM) the ocean component of the MPI-Earth system model, *J. Adv. Model. Earth Syst.,* **5,** 422–446.

Klemann, V., Martinec, Z. & Ivins, E.R., 2008. Glacial isostasy and plate motion, *J. Geodyn.,* **46**(3–5), 95–103.

König, R., Fagiolini, E., Raimondo, J. & Vei, M., 2018. A non-tidal atmospheric loading model: on its quality and impacts on orbit determination and C20 from SLR, in *International Symposium on Earth and Environmental Sciences for Future Generations : Proceedings of the IAG General Assembly, Prague, Czech Republic, June 22- July 2, 2015, (International Association of Geodesy Symposia ; 147),* pp. 189–194. eds Freymueller, J.T. & Sánchez, L., Springer.

Nastula, J., Gross, R. & Salstein, D. A., 2012. Oceanic excitation of polar motion: Identification of specific oceanic areas important for polar motion excitation, *J. Geodyn.,* **62,** 16–23.

Petit, G. & Luzum, B., 2010. IERS Conventions 2010, IERS Tech. Note, 36, International Earth rotation and reference systems service, Verlag des Bundesamts für Kartographie und Geodäsie.

Quinn, K.J., Ponte, R.M. & Tamisiea, M.E., 2015. Impact of self-attraction and loading on Earth rotation, *J. geophys. Res.,* **120,** 4510–4521.

Rickard, G.J., Lunnon, R.W. & Tenenbaum, J., 2001. The Met Office upper air winds: Prediction and verification in the context of commercial aviation data, *Meteorol. Appl.,* **8,** 351–360.

Salstein, D.A. & Rosen, R.D., 1997. Global momentum and energy signals from reanalysis systems, in *7th Conf. on Climate Variations,* pp. 344–348, American Meteorological Society, Boston, MA.

Schindelegger, M., Böhm, J., Salstein, D. & Schuh, H., 2011. High-resolution atmospheric angular momentum functions related to Earth rotation parameters during CONT08, *J. Geod.,* **85,** 425–433.

Tamisiea, M.E., Hill, E.M., Ponte, R.M., Davis, J.L., Velicogna, I. & Vinogradova, N.T., 2010. Impact of self-attraction and loading on the annual cycle in sea level, *J. geophys. Res.,* **115**(C7), 1–15.

Yan, H. & Chao, B.F., 2012. Effect of global mass conservation among geophysical fluids on the seasonal length of day variation, *J. geophys. Res.,* **117,** B02401, doi:10.1029/2011JB008788.

Yu, N., Li, J., Ray, J. & Chen, W., 2018. Improved geophysical excitation of length-of-day constrained by Earth orientation parameters and satellite gravimetry products, *Geophys. J Int.,* **214**(3), 1633–1651.

Zhang, X., Jin, S. & Lu, X., 2017. Global surface mass variations from continuous GPS observations and satellite altimetry data. *Remote Sens.,* **9**(10), doi:10.3390/rs9101000.

Zhou, Y.H., Chen, J.L., Liao, X.H. & Wilson, C.R., 2005. Oceanic excitations on polar motion: a cross comparison among models, *Geophys. J. Int.,* **162,** 390.

Zhou, Y.H., Salstein, D.A. & Chen, J.L., 2006. Revised atmospheric excitation function series related to variable rotation under consideration of surface topography, *J. geophys. Res.,* **111,** D12108, doi:10.1029/2005JD006608.